Cell Metabolism, Volume *32*

Supplemental Information

Oligodendrocytes Provide Antioxidant Defense Function for Neurons by Secreting Ferritin Heavy Chain

Chaitali Mukherjee, Tina Kling, Belisa Russo, Kerstin Miebach, Eva Kess, Martina Schifferer, Liliana D. Pedro, Ulrich Weikert, Maryam K. Fard, Nirmal Kannaiyan, Moritz Rossner, Marie-Louise Aicher, Sandra Goebbels, Klaus-Armin Nave, Eva-Maria Krämer-Albers, Anja Schneider, and Mikael Simons

SUPPLEMENTARY FIGURES

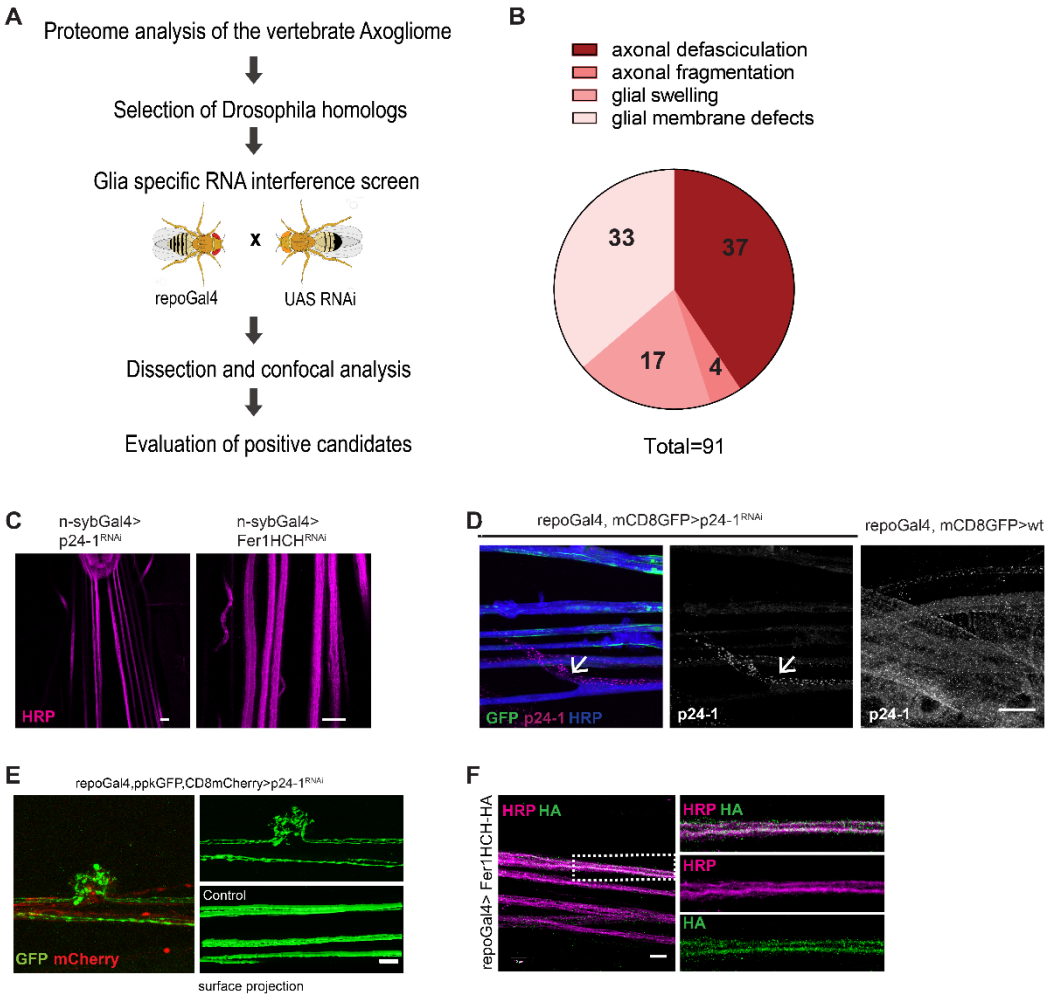

Figure S1 - Glial-specific RNAi screen in *Drosophila* - related to Figure 1

(A) Schematic depicts the experimental work flow employed for the candidate selection and further analysis of glia-specific RNA interference screen in *Drosophila Melanogaster*.

(B) Quantification of positive candidates sorted by neuronal and glial defects. Drosophila RNAi of the selected candidates were expressed with the glial-specific repoGal4 driver line. Third instar larval peripheral nervous system was scored after confocal analysis for morphological changes using CD8-GFP to detect glia and antibodies against HRP and Futsch to visualize the neuronal membrane and cytoskeleton, respectively.

(C) Representative image depicting *p24-1* RNAi (left panel) and *Fer1HCH* RNAi (right panel) silencing in neurons using the driver line *n-sybGal4*. Immunostaining against HRP shows intact nerves without axonal protrusions. Scale=20µm.

(D) Left panel, representative images using *repoGal4*-driven CD8-GFP to visualize glia (green), and against HRP to label neuronal membrane (blue), together with antibodies against

anti-p24-1 (magenta). RNAi-mediated silencing of p24-1 in glia abolishes p24-1 immunostaining in the peripheral nerves, but not in neighboring non-neuronal tissue (marked with an arrow in the left and middle panel). Right panel, p24-1 immunostaining is shown in the peripheral nervous system of control flies without p24-1 silencing. Scale=20µm.

(E) Image showing single axons labeling with local degeneration after p24-1 RNAi in glia. Glial membrane was visualized by *repoGal4*-driven CD8-GFP (red) and axons by *ppk-GFP* expression (green), which labels 2 to 4 axons per nerve. Scale bar=10 µm.

(F) Representative images depict the localization of HA-Fer1HCH when expressed with the pan-glial driver line *repoGal4*. HA-Fer11HCH protein was detected with the HA antibody (green) while neurons were labeled with the HRP antibody (magenta). Neighboring panel represent higher magnification image of indicated part (white box). Scale=30µm.

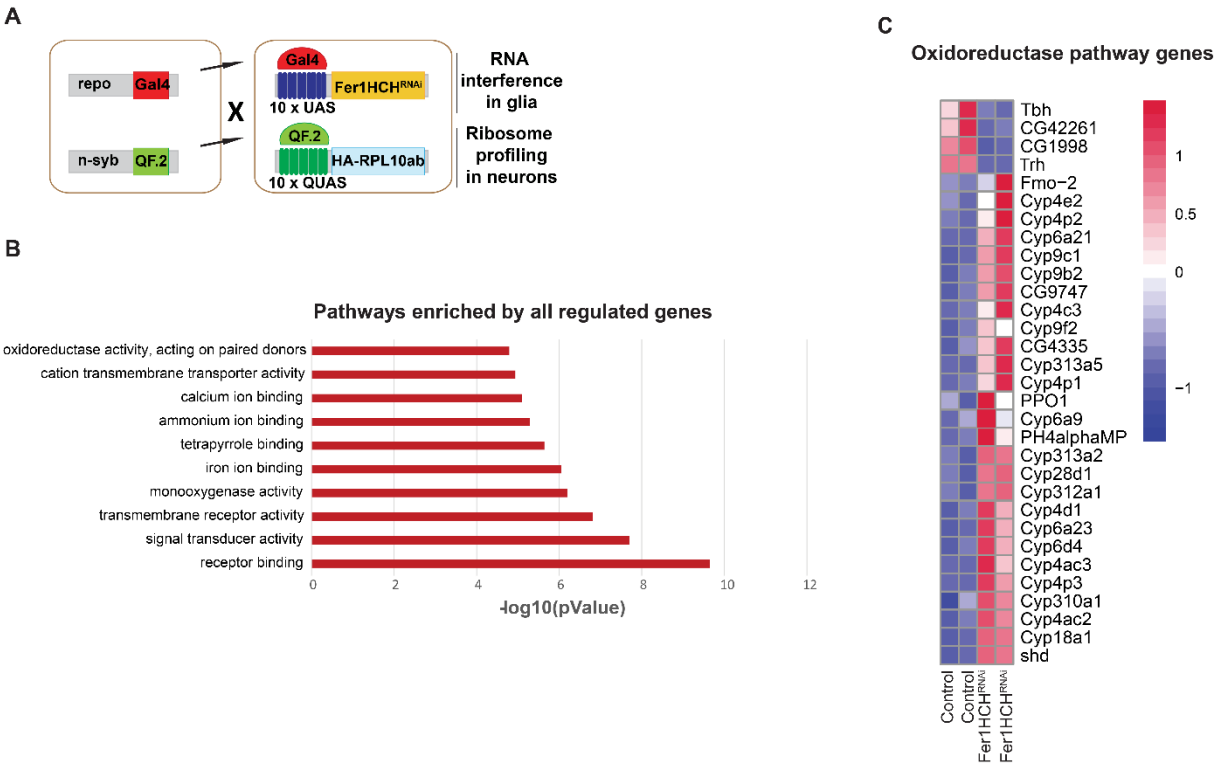

Figure S2 - RNAi-mediated silencing of Fer1HCH in glia affects oxidoreductase activity in neurons - related to Figure 2

(A) Schematic representation of ribosome profiling strategy of neurons after glial-specific knockdown of *Fer1HCH*. For ribosome profiling we used transgenic flies expressing the ribosomal protein Rpl10ab-HA under the pan-neuronal driver *n-syb* in combination with *Repo-Gal4;UAS-Fer1hch*^{RNAi} as depicted.

(B) Pathway analysis of the 1485 differentially (2-fold, p value 0.05) genes in neurons after glial-specific knockdown of Fer1HCH.

(C) Heat map indicates the significantly up- (red) or down- (blue) regulated genes linked to the oxidoreductase pathway in control neurons (Control) as compared to neurons after glial-specific knockdown of Fer1HCH (*Fer1HCH*^{RNAi}).

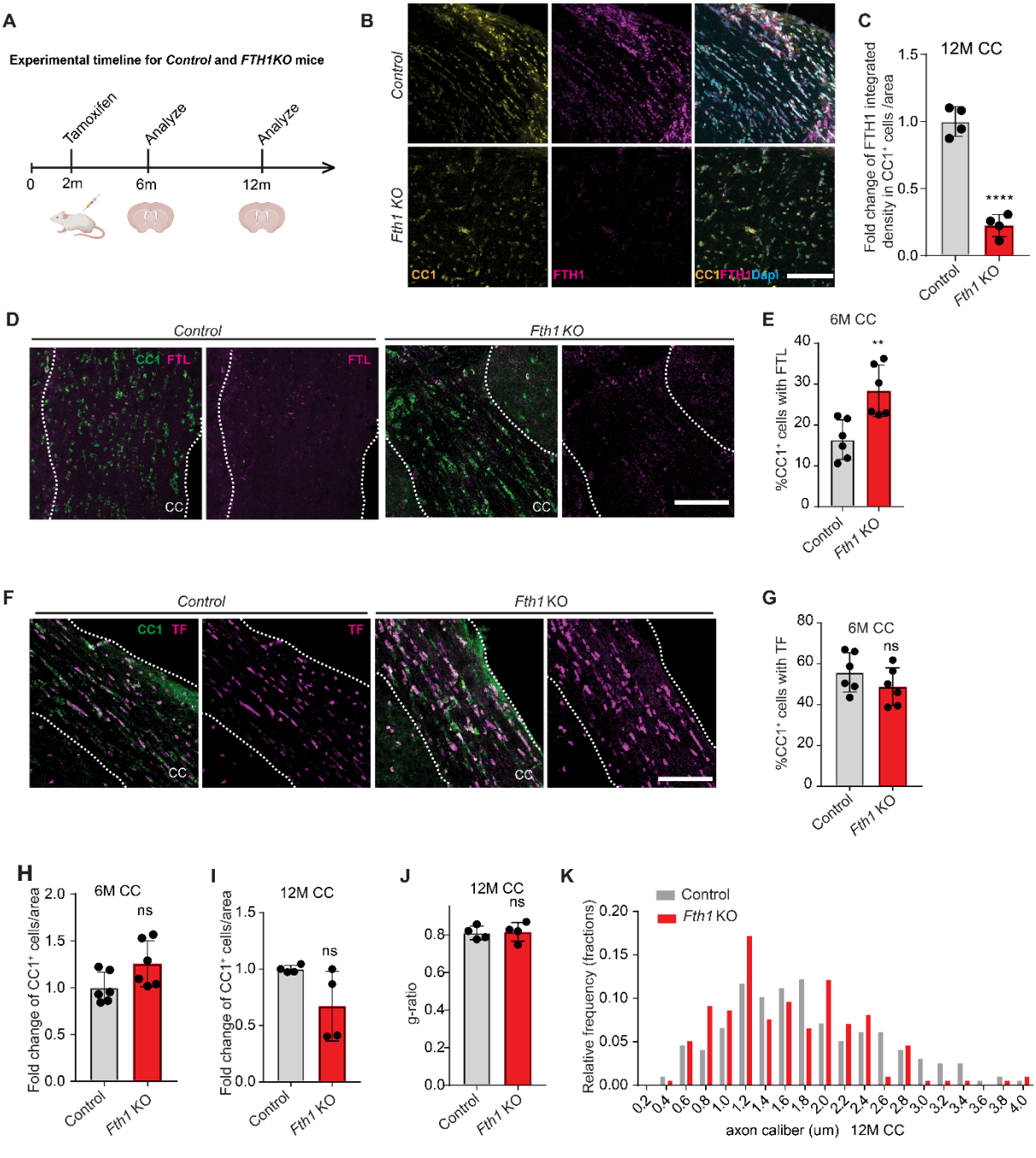

Figure S3 - Characterization of oligodendrocyte-specific ferritin heavy chain knockout mice - related to Figure 5

(A) Schematic depicts the experimental work flow used for inducing the conditional knockout of FTH1 and subsequent time points for analyses. Control and *FTH1* KO mice were both injected with tamoxifen at 2 months of age, followed by histological analysis at 6 and 12 months of age.

(B) Images of corpus callosum of 12 month old control ($Fth1^{fl/fl}$;$PLP^{wt/wt}$) and *Fth1* KO ($Fth1^{fl/fl}$;$PLP^{CreERT2/wt}$) mice immunostained with antibodies against FTH1 (magenta) and CC1 (yellow) 10 months after tamoxifen treatment. Scale=100µm.

(C) Quantification of integrated density of FTH1 immunostaining within $CC1^+$ cells/area. Data are represented as fold change, and all values are normalized to the mean of control mice.

(D) Images of corpus callosum of 6-month-old control and *Fth1* KO mice immunostained with antibodies against ferritin light chain (FTL) (magenta) and CC1 (green). Scale=100µm.

(E) Quantification of percentage of $CC1^+$ cells expressing FTL in the corpus callosum, and are shown as mean ± SD; ns=non-significant, **P<0.01, by two-tailed Student´s t-test.

(F) Images of corpus callosum of 6-month-old control and *Fth1* KO mice immunostained with antibodies against transferrin (TF; magenta) and CC1 (green). Scale=100µm.

(G) Quantification of percentage of $CC1^+$ cells expressing TF in the corpus callosum.

(H, I) Quantification of density of $CC1^+$ oligodendrocytes in the corpus callosum (CC) of 6 months (I) and 12 months (J) old *Fth1* KO and control mice. Data are represented as fold change, and all values are normalized to the mean of control mice.

(J) Quantification of myelin thickness as measured by g-ratios (axon diameter divided by fiber diameter) for corpus callosum axons of *Fth1* KO and control mice at 12 months of age (10 months after tamoxifen).

(K) Graphical representation of axonal caliber distribution for corpus callosum axons of 12 month old *Fth1* KO (red) and control mice (grey).

(C, E, G, H, I, J, K) Data are represented as fold change, and all values are normalized to the mean of control mice. All data are shown as mean ± SD; ns=non-significant, *P<0.05, **P<0.01, ****P<0.0001 by two-tailed Student´s t-test.

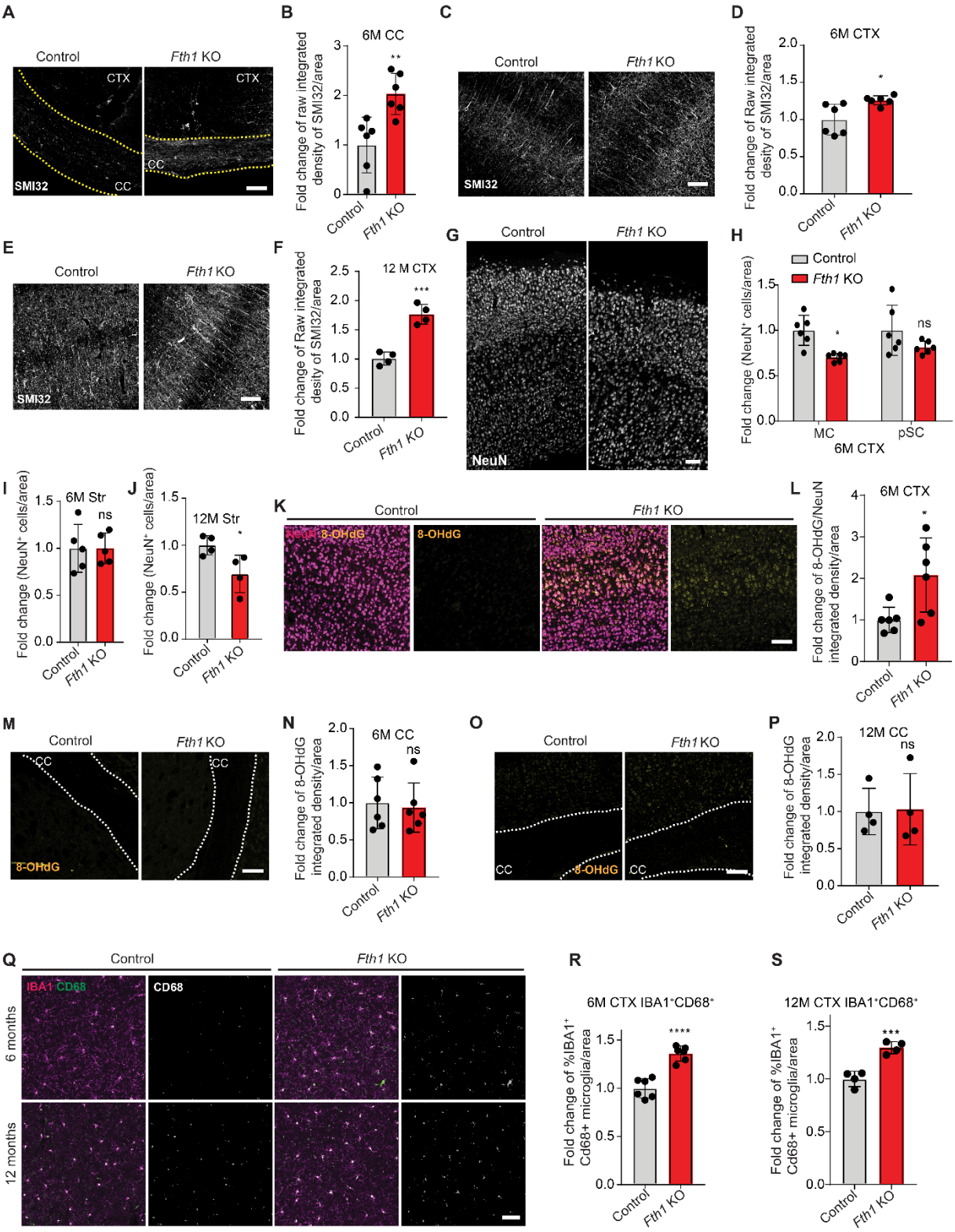

Figure S4 - Oligodendrocyte-specific ferritin heavy chain knockout results in neuronal loss in mice - related to Figure 5

(A) Images of corpus callosum of 6 months old control ($Fth1^{fl/fl}$;$PLP^{wt/wt}$) and *Fth1* KO ($Fth1^{fl/fl}$;$PLP^{CreERT2/wt}$) mice immunostained with antibodies against unphosphorylated neurofilament (SMI32) 4 months after tamoxifen treatment. Scale=100µm.

(B) Quantification of relative SMI32 integrated density per area for 6 months old *Fth1* KO (red bar) and control (grey bar) mice. Data are represented as fold change, and values are normalized to mean of control mice.

(C, E) Images of neocortex of 6 months (C) and 12 months (E) old control and *Fth1* KO mice immunostained with antibodies against unphosphorylated neurofilament (SMI32), 4 and 10 months after tamoxifen treatment. Scale=100µm.

(D, F) Quantification of relative SMI32 integrated density per area in the cortex for 6 months and 12 months old *Fth1* KO (red bar) and control (grey bar) mice. Data are represented as fold change, and values are normalized to mean of control mice.

(G) Images of neocortex of 6 months old control and *Fth1* KO mice immunostained with antibodies against neuronal nuclei (NeuN). Scale=100µm.

(H) Quantification of relative density of $NeuN^+$ cells/area of 6 months old *Fth1* KO (red) and control (grey) mice motor (MC) and primary sensory cortex (pSC). Data are represented as fold change, and values are normalized to mean of control mice and are Data are means ± SD; ns=non-significant, *$p<0.05=0.011$ by two way ANOVA test with Sidak's for multiple comparison test.

(I, J) Quantification of relative density of $NeuN^+$ cells/area of 6 months old *Fth1* KO (red) and control (grey) mice striatum (Str) at 6 months and 12 months of age. Data are represented as fold change, and values are normalized to mean of control mice.

(K) Images of neocortex of 6 months old control and *Fth1* KO mice immunostained with antibodies against oxidative DNA modifications (8-OHdG, yellow), and NeuN (magenta). Scale=100µm.

(L) Quantification of relative 8-OHdG integrated density per $NeuN^+$ area in 6 months old *Fth1* KO (red) and control mice (grey). Data are represented as fold change, and values are normalized to mean of control mice.

(M, O) Images of corpus callosum of 6 months (M) and 12 months (O) old control and *Fth1* KO mice immunostained with antibodies against oxidative DNA modifications (8-OHdG, yellow). Scale=100µm.

(N, P) Quantification of relative 8-OHdG integrated density per area in the corpus callosum of 6 months and 12 months old *Fth1* KO (red) and control mice (grey). Data are represented as fold change, and values are normalized to mean of control mice.

(Q) Images showing immunostaining against IBA1 (magenta) and CD68 (green) in the cortex of 6 months (upper panels) and 12 months (lower panels) old control and *Fth1* KO mice. Scale=100µm.

(R, S) Quantification of the percentage of IBA1 positive for CD68 per area. Data are represented as fold change, and values are normalized to mean of control animals.

All data in are shown as mean ± SD; ns=non-significant *p<0.05, **p<0.01, ***p<0.001, ****p<0.0001 by two-tailed Student´s t-test.

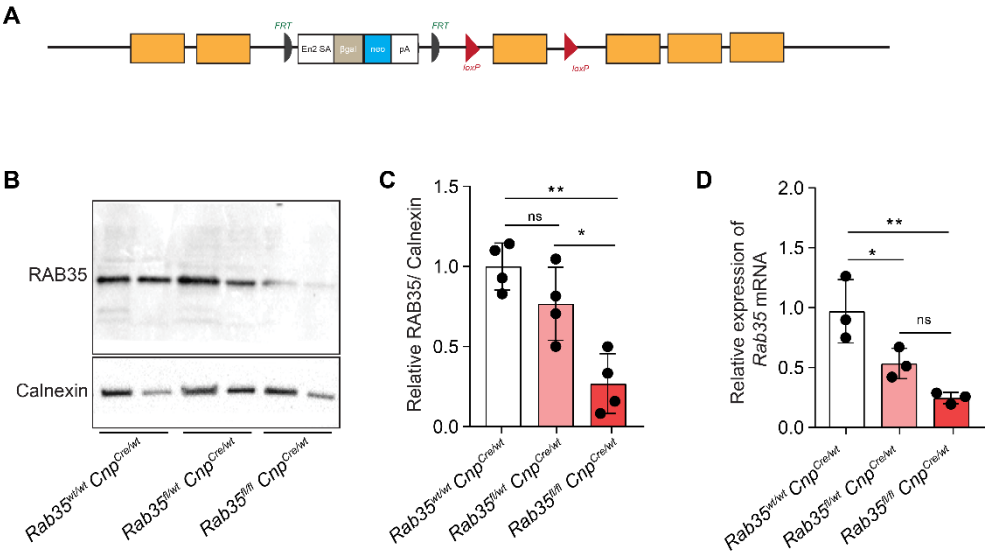

Figure S5 - Generation of conditional Rab35 knockout mice - related to Figure 7

(A) ES clone for conditional allele. The structure of the retroviral gene trap that was used to disrupt the *Rab35* gene is shown with the splice acceptor (En2 SA), the lacZ reporter (lacZ), the neomycin resistance gene (neo) and the polyadenylation consensus site (pA). FLP recognition (Frt) sites are represented in grey and the loxP sites in red.

(B) Immunoblot for Rab35 and loading control (Calnexin) from cerebellar homogenates from mice of indicated genotypes.

(C) Quantification of relative amounts of RAB35 in cerebellar lysates from $Rab35^{wt/wt}$; $Cnp^{Cre/wt}$ (white), $Rab35^{fl/wt}$;$Cnp^{Cre/wt}$ (pink) and *Rab35* KO mice (red; $Rab35^{fl/fl}$;$Cnp^{Cre/wt}$). Quantification of RAB35 protein quantification normalized to Calnexin.

(D) Relative expression of *Rab35* mRNA levels in cerebellum homogenates. Quantification of relative amounts of *Rab35* mRNA in cerebellar lysates from $Rab35^{wt/wt}$; $Cnp^{Cre/wt}$ (white), $Rab35^{fl/wt}$;$Cnp^{Cre/wt}$ (pink) and *Rab35* KO mice (red; $Rab35^{fl/fl}$;$Cnp^{Cre/wt}$). All data are means ± SD; *p<0.05, ** p<0.01 by one way ANOVA test with Tukey's multiple comparison test.

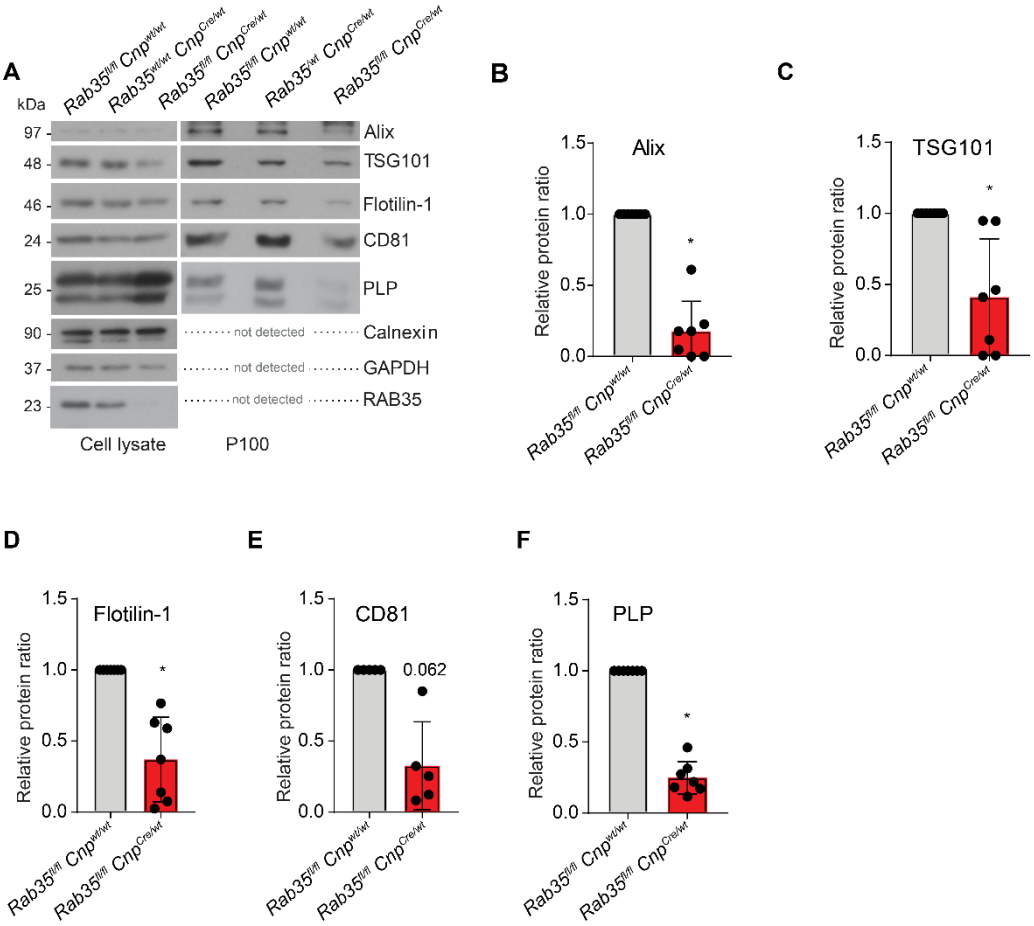

Figure S6 - Reduced secretion of EV into culture medium of Rab35 knockout oligodendrocytes - related to Figure 7

(A) Medium was collected from primary cultures of oligodendrocytes and submitted to sequential centrifugation steps. Cell lysates and the resulting 100,000g pellets were analyzed by Western blotting for Alix, TSG101, Flotilin-1, CD81, PLP, Calnexin, GAPDH and RAB35.

(B-F) Quantification are shown for *Rab35* KO ($Rab35^{fl/fl}$;$Cnp^{Cre/wt}$) mice (red) normalized to $Rab35^{fl/fl}$;$Cnp^{wt/wt}$ (grey). All data shown as mean ± SD; *$p<0.05$, by Wilcoxon matched-pairs signed rank test.

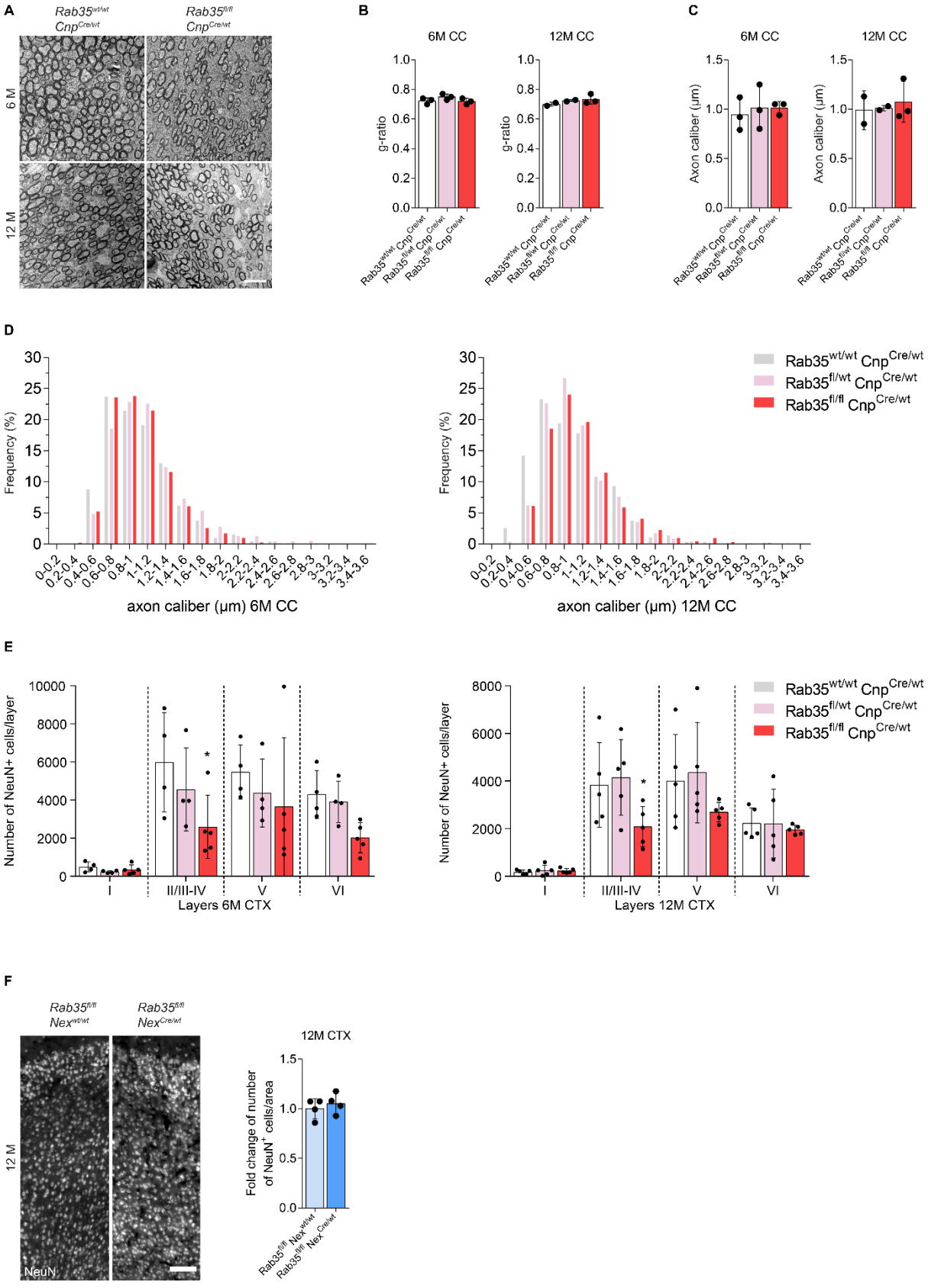
A
Rab35wt/wt Cnp Cre/wt
Rab35fl/fl Cnp Cre/wt
6 M
12 M
B
6M CC
12M CC
g-ratio
C
6M CC
12M CC
Axon caliber (µm)
D
Frequency (%)
axon caliber (µm) 6M CC
axon caliber (µm) 12M CC
Rab35wt/wt Cnp Cre/wt
Rab35fl/wt Cnp Cre/wt
Rab35fl/fl Cnp Cre/wt
E
Number of NeuN+ cells/layer
I
II/III-IV
V
VI
Layers 6M CTX
Layers 12M CTX
F
Rab35fl/fl Nexwt/wt
Rab35fl/fl Nex Cre/wt
12 M
NeuN
12M CTX
Fold change of number of NeuN+ cells/area
Rab35fl/fl Nexwt/wt
Rab35fl/fl Nex Cre/wt

Figure S7- Conditional deletion of Rab35 in oligodendrocytes does not affect myelination and leads to neuron loss and oxidative injury- related to Figure 7

(A) Electron micrograph images of corpus callosum brain sections from 6 and 12 months old oligodendrocyte-specific *Rab35* knockout ($Rab35^{fl/fl}$;$Cnp^{Cre/wt}$) and control mice ($Rab35^{wt/wt}$; $Cnp^{Cre/wt}$). Scale=2.5 μm.

(B) Quantification of g-ratio of $Rab35^{wt/wt}$;$Cnp^{Cre/wt}$ (white), $Rab35^{fl/wt}$;$Cnp^{Cre/wt}$ (pink) and *Rab35* KO mice (red) at 6 and 12 months. All data are means ± SD; analyzed by one way ANOVA test with Tukey's multiple comparison test.

(C) Quantification of axon caliber of $Rab35^{wt/wt}$;$Cnp^{Cre/wt}$ (white), $Rab35^{fl/wt}$;$Cnp^{Cre/wt}$ (pink) and *Rab35* KO mice (red) at 6 and 12 months. All data are means ± SD.

(D) Quantification of axon caliber distribution of $Rab35^{wt/wt}$;$Cnp^{Cre/wt}$ (white), $Rab35^{fl/wt}$;$Cnp^{Cre/wt}$ (pink) and *Rab35* KO mice (red) at 6 and 12 months. All data are means; analyzed by one way ANOVA test with Tukey's multiple comparison test.

(E) Quantification of fold change of the number of $NeuN^+$ cells in each cortical layer of 6 and 12 months old $Rab35^{wt/wt}$;$Cnp^{Cre/wt}$ (white), $Rab35^{fl/wt}$;$Cnp^{Cre/wt}$ (pink) and *Rab35* KO mice (red). All data are means ± SD; *$p<0.05$ by one-way ANOVA test with Tukey's multiple comparison test.

(F) Left: Images of 12 months old control ($Rab35^{fl/fl}$;$Nex^{wt/wt}$) and Rab35 KO ($Rab35^{fl/fl}$;$Nex^{Cre/wt}$) mice motor cortex. Scale bar: 100 μm. Right: Quantification of fold change of the number of $NeuN^+$ cells/area of 12 month old $Rab35^{fl/fl}$;$Nex^{wt/wt}$ (light blue) and $Rab35^{fl/fl}$;$Nex^{Cre/wt}$ mice (blue). Data are means ± SD; analyzed by two-tailed Student´s t-test.

Table S2 - Table listing genes that resulted an axonal phenotype when knocked down in glia-related to Figure 1 and Figure S1.

Identified Proteins	Drosophilla Gene	Axonal defasciculation	Axonal fragmentation
a disintegrin and metallopeptidase domain 23	Kul	x	
protein tyrosine phosphatase, receptor type, D	ptpmeg, isoform D	x	
Adam22 protein	mind-meld, isoform D	x	
unnamed protein product	syntaxin 7	x	
ectonucleoside triphosphate diphosphohydrolase 2	NTPase, isoform D	x	
transferrin receptor protein 1	goliath	x	
unnamed protein product	CG10320	x	
ADP/ATP translocase 2	stress-sensitive B, ADP/ATP translocase	x	
mCG10343, isoform CRA_c	mitochondrial phosphate carrier protein	x	
mCG10343, isoform CRA_c	CG9090	x	
putative membrane associated progesterone receptor component	membrane steroid binding protein	x	
synaptotagmin-1	Synaptotagmin 1	x	
carnitine palmitoyltransferase 1a, liver, isoform CRA_b	CPTI	x	
guanosine diphosphate (GDP) dissociation inhibitor 1, isoform CRA_a	GDP dissociation inhibitor	x	
mCG20085, isoform CRA_a [Mus musculus]	Kua	x	
mitochondrial import inner membrane translocase subunit TIM50 precursor	tiny tim 50	x	
mitochondrial import receptor subunit TOM22 homolog	maggie	x	
Psmd1 protein	Rpn2		x
Bcl-2-like protein 13 (apoptosis facilitator)	death executioner Bcl-2 homologue	x	
Vesicle-associated membrane protein-associated protein B	Vap-33-1	x	
reticulon 1, isoform CRA_b	CG17221	x	
UBX domain containing 8, isoform CRA_a	Fas-associated factor	x	

unnamed protein product	CG3409	x	
solute carrier family 12 member 2	sodium chloride cotransporter 69	x	
mCG10343, isoform CRA_c	mitochondrial phosphate carrier protein	x	
AMPA selective glutamate receptor	glutamate receptor subunit kainate subtype	x	
Glutamate Recepor subunit	CG3822	x	
inositol 1,4,5-triphosphate receptor 1, isoform CRA_b	Itp-r83A	x	x
integrin alpha-6 isoform a precursor	inflated	x	
hCG2002731, isoform CRA_e	multiple edematous wings, isoform B	x	
integrin alpha-2 precursor	CG7739	x	
leucine-rich repeat and fibronectin type-III domain-containing protein 4 precursor	kekkon-1		x
multiple epidermal growth factor-like domains protein 10 precursor	CG7466	x	
neurotrophic tyrosine kinase, receptor, type 2, isoform CRA_d	bent	x	
unnamed protein product	roundabout 2	x	
unnamed protein product	CG34114	x	
Transmembrane emp24 domain-containing protein 7	p24-related-1		x
amyloid precursor-like protein 1	appl	x	
olfactomedin 1, isoform CRA_a	CG6867	x	
sphingomyelin phosphodiesterase 1, acid lysosomal (acid sphingomyelinase), isoform CRA_b	CG3376	x	